Squeezed and fragmented states of strongly interacting bosons in a double well. Part I: Theoretical models

Joel C. Corbo,[1,2,*] Jonathan L. DuBois,[3] and K. Birgitta Whaley[1,4]

[1] *Berkeley Center for Quantum Information and Computation, University of California, Berkeley, CA 94720, USA*
[2] *Department of Physics, University of California, Berkeley, CA 94720, USA*
[3] *Lawrence Livermore National Lab, 7000 East Ave, L-415, Livermore, CA 94550, USA*
[4] *Department of Chemistry, University of California, Berkeley, CA 94720, USA*

(Dated: April 9, 2014)

We present a systematic study of the phenomena of squeezing and fragmentation for a Bose-Einstein condensate (BEC) in a three dimensional double well potential over a range of interaction strengths and barrier heights. We analyze the properties of the condensate in the context of both a standard and an improved two-mode model and a recently-proposed eight-mode model. One fundamental difference between this and previous two-mode work is that we explicitly examine well geometries that exhibit appreciable overlap in the one-body wavefunctions localized in the left and right wells rather than assuming that they are nearly isolated from each other. One particularly surprising observation that we have made in our study of these models is the existence of an interaction strength that maximizes squeezing, which is in stark contrast to the predictions of the two-mode model with no overlap between the wells for which squeezing monotonically increases with interaction strength. We explain this and other novel results through a careful study of the ground state properties produced by various terms in the model Hamiltonians and the relationship between the strength of these terms and the system parameters, such as well geometry and atomic interaction strength.

PACS numbers: 67.85.Bc, 03.75.Hh

arXiv:1404.2250v1 [cond-mat.quant-gas] 8 Apr 2014

I. INTRODUCTION

Since the achievement of Bose-Einstein condensation in the laboratory [1, 2], there has been significant interest, both experimental and theoretical, in the study of a BEC in a double well trap. To date, the problem of cold atoms in a double well potential has been modeled extensively within a two-mode approximation, in which the many-body state of the system is computed in terms of the two lowest energy one-body states of the system [3–11]. As discussed in [5], this approach is generally restricted to the limit of weak particle interactions. Furthermore, of the studies listed here only [10, 11] considered effects beyond the usual one-body tunneling (J) and on-site interaction (U) terms (i.e., they included two-body tunneling terms). Recent theoretical work on understanding the double well in the context of an eight-mode approximation [12] has uncovered some deficiencies of the two-mode model. In particular, it was shown that even in regimes where one might naively expect only the lowest two single particle modes to contribute based on energy arguments, the ground state can nevertheless contain components of higher modes. Such admixtures have the potential to dramatically influence the collective properties of the system.

One such property is the degree of *number squeezing* exhibited by the many-body wavefunction of the system. Number squeezing is related to the probability of finding particular values for the difference in the number of atoms on the two sides of the double well. In an unsqueezed system, the probabilities are distributed like a Gaussian centered on a difference of zero; in other words, while the most probable configuration is the one with an equal number of particles on each side of the barrier, there is non-negligible probability of finding other configurations. A system is said to be squeezed when this distribution narrows, so that the probability of observing a difference of zero dominates over all other possibilities. In general, the amount of squeezing a system exhibits depends on the strength of the interactions between the particles, because interactions can enhance or suppress the fluctuation of atoms across the barrier. Of the two-mode studies cited above, only [5, 6] explicitly considered squeezing, while this phenomenon has not yet been addressed within the eight-mode model. However, squeezing has implications for a number of important practical problems, including the design of more precise atom interferometers [13, 14].

The symmetry of the double well potential also allows for *fragmentation* [15]. In a canonical BEC, we can express the system's many-body wavefunction in such a way that all of the particles are in the same one-body state. However, under the right conditions, the BEC can exhibit fragmentation, in which multiple one-body states are macroscopically occupied by the particles in the condensate. When population is further distributed over single-particle states with non-macroscopic occupa-

* Email: joel.corbo@colorado.edu; Current affiliation: Center for STEM Learning, University of Colorado Boulder, Boulder, CO 80309

tion, the BEC is said to be *depleted*. Much theoretical effort has gone into understanding fragmentation using two-mode models [16, 17], including studies of fragmentation in a double well [7–9]. As is the case with squeezing, these models are inadequate to fully capture the behavior of the system with respect to fragmentation at large interaction strengths. Fragmentation and depletions have also not yet been studied within the eight-mode model.

This paper is the first in a series of two papers in which we undertake a systematic study of the phenomena of squeezing and fragmentation for a Bose-Einstein condensate in a three dimensional double well potential over a range of interaction strengths and barrier heights. In this first paper, we conduct the analysis of these properties in the context of the two- and eight-mode models, extending the scope of these models as required. These studies provide a reference point for the analysis of squeezing and fragmentation with numerically exact quantum Monte Carlo methods that will be presented in the second paper of this series [18]. However they also provide new information within the restricted domain of the two- and eight-mode models. In particular, unlike all previous finite mode calculations which assume no appreciable overlap between one-body wave functions localized in left and right wells (equivalently, near degeneracy of the lowest two modes), we explicitly examine well geometries that allow such overlap and show that this gives rise to a non-monotonic dependence of squeezing on interaction strength.

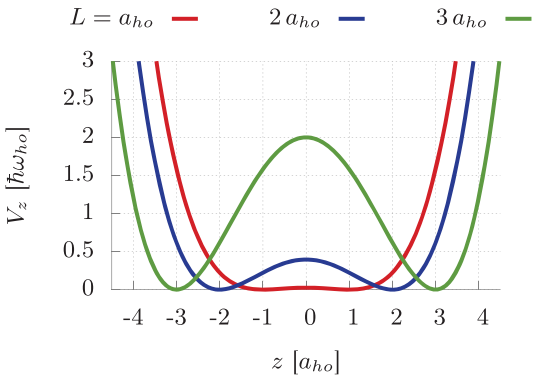

Figure 1. (Color online) The z part of the external potential for $\alpha = 4/81\,a_{ho}^{-2}$. The height of the barrier, $V_{ext}(0) = m\omega_{ho}^2\alpha L^4/2$, is $2/81\,\hbar\omega_{ho}$, $32/81\,\hbar\omega_{ho}$, and $2\,\hbar\omega_{ho}$ for $L = a_{ho}$, $2\,a_{ho}$, and $3\,a_{ho}$, respectively.

	Energy $[\hbar\omega_{ho}]$				
$L\ [a_{ho}]$	$\phi_0(z)$	$\phi_1(z)$	$\phi_2(z)$	$\phi_3(z)$	$V_{ext}(0)$
1	0.167	0.594	1.220	1.946	0.025
2	0.297	0.482	1.026	1.614	0.395
3	0.634	0.637	1.681	1.801	2

Table I. Energies of the ground and first three excited states of the z part of the double well potential, as well as the energy of the double well barrier for $\alpha = 4/81\,a_{ho}^{-2}$ and various L. Note that these energies do not include the contribution from the x and y parts of the state.

II. THE SYSTEM

A. The Many-Body Double Well Hamiltonian

The many-body Hamiltonian for N bosons of mass m interacting pairwise in an external potential has the form

$$\hat{H} = \sum_{j=1}^{N}\left(-\frac{\hbar^2}{2m}\nabla_j^2 + V_{ext}(\mathbf{r}_j)\right) + \sum_{j<k}^{N} V_{int}(\mathbf{r}_j, \mathbf{r}_k). \quad (1)$$

For the external potential, we use a three-dimensional double well potential of the form

$$V_{ext}(\mathbf{r}) = \frac{1}{2}m\omega_{ho}^2\left(x^2 + y^2 + \alpha\left(z^2 - L^2\right)^2\right), \quad (2)$$

where ω_{ho} is the characteristic harmonic trap frequency in the xy plane, α characterizes the height of the barrier between wells at $z = 0$, and $2L$ is the distance between the minima of the wells (see Fig. 1). Table I lists the energies of the first four states of the double well to give a sense of where they lie relative to the height of the barrier. These states will be relevant to constructing models for the double well system in Sec. III.

We use the experiment described in [19] to give a realistic sense of the magnitude of the parameters of the external potential. This experiment used ^{23}Na atoms and a trap with $L = 6.5\,\mu$m, $\omega_{ho}/2\pi = 615\,$Hz, and $\frac{1}{2}m\omega_{ho}^2\alpha L^4 = h \times 4.7\,$kHz (equivalently, $\alpha = 6.1 \times 10^{-9}\,\mathrm{nm}^{-2}$). We present our results in terms of the system's characteristic length $a_{ho} = (\hbar/m\omega_{ho})^{1/2}$ and energy $\hbar\omega_{ho}$. For [19], $a_{ho} = 845\,$nm and $\hbar\omega_{ho} = 2.54\,$peV, so $L = 7.7\,a_{ho}$ and $\alpha = 0.26\,a_{ho}^{-2}$, which are comparable to the values in the systems we simulate.

Because we are interested in ground state (i.e., low energy) properties, we assume s-wave scattering and hence use a hard sphere interaction potential:

$$V_{int}(r_{jk}) = \begin{cases} \infty & r_{jk} \le a \\ 0 & r_{jk} > a \end{cases}, \quad (3)$$

where $r_{jk} = |\mathbf{r}_j - \mathbf{r}_k|$ and a is the (positive) s-wave scattering length, which determines the effective interaction strength.

B. The Differential Number Distribution and Squeezing

We are primarily interested in understanding the relationship between number squeezing and particle interaction strength. The differential number distribution is related to the operator $\hat{n} = \frac{1}{2}(\hat{L} - \hat{R})$, where $\hat{L}$ is given

in the position representation by

$$\hat{L} = \sum_{i=1}^{N} \begin{cases} 1 & z_i < 0 \\ 0 & z_i > 0 \end{cases}, \tag{4}$$

and $\hat{R}$ is given by the analogous expression. For a completely symmetric state $\Psi(\mathbf{r}_1, \ldots, \mathbf{r}_N)$, we find

$$\langle \Psi | \hat{L} | \Psi \rangle = N \int_{-\infty}^{0} \left[\int_{-\infty}^{\infty} \int_{-\infty}^{\infty} |\Psi_1(\mathbf{r}_1)|^2 dx_1 dy_1 \right] dz_1, \tag{5}$$

where

$$|\Psi_1(\mathbf{r}_1)|^2 = \int_{-\infty}^{\infty} \cdots \int_{-\infty}^{\infty} |\Psi(\mathbf{r}_1, \ldots, \mathbf{r}_N)|^2 d\mathbf{r}_2 \cdots d\mathbf{r}_N, \tag{6}$$

and similarly for $\langle \Psi | \hat{R} | \Psi \rangle$. Intuitively, $\hat{L}$ and $\hat{R}$ measure the fraction of the probability density of the many-body state that exists in the left and right wells, respectively.

Because of the symmetry of the double well potential, the ground state of the system has $\langle \Psi | \hat{L} | \Psi \rangle = \langle \Psi | \hat{R} | \Psi \rangle = N/2$ (and hence $\langle \Psi | \hat{n} | \Psi \rangle = 0$) regardless of the strength of the interaction between the particles. However, the width of this distribution, characterized by its standard deviation $\sigma_n = \sqrt{\langle \Psi | \hat{n}^2 | \Psi \rangle}$, does vary with a. For the noninteracting ($a = 0$) case, the many-body ground state consists of a product of single-particle ground states, and $\sigma_n = \sqrt{N}/2$. For a repulsive interaction ($a > 0$), we expect that the number distribution will narrow because configurations with many particles on one side of the double well and few on the other will be energetically disfavored relative to configurations that more evenly split the particles between the two sides. This narrowing is what is meant by number squeezing. We define a squeezing parameter S to characterize the amount of squeezing in the system relative to the non-interacting ground state:

$$\begin{aligned} S &= 1 - \frac{\sigma_n^2}{N/4} \\ &= 1 - \frac{1}{N} \langle \Psi | (\hat{L} - \hat{R})^2 | \Psi \rangle . \end{aligned} \tag{7}$$

$S = 0$ corresponds to no squeezing, and $S = 1$ corresponds to a fully squeezed state, in which $\sigma_n = 0$.

Based on this qualitative argument, we would expect squeezing to increase with interaction strength. This is indeed the prediction of the two-mode mean-field model when the two wells are well-separated [5], but as we shall see below, it fails to hold when this condition isn't met. Additionally, the results of the eight-mode model also disagree with this simple picture.

C. The One Body Density Matrix, Fragmentation, and Depletion

We analyze additional condensate properties by computing and diagonalizing the one body density matrix (OBDM) which is a valid description of the BEC at all densities and interaction strengths [20, 21]. This computation allows us to determine the fraction of particles that are part of the BEC and the state(s) they occupy, i.e., the extent of depletion and fragmentation, as a function of interaction strength. This provides another way to understand the breakdown of the mean-field models.

In a non-interacting system, the condensate is defined in terms of a single-particle ground state wavefunction, and the condensate fraction is the ratio of the number of particles occupying that state to the total number of particles. For a uniform system, momentum is a good quantum number, and the condensate is associated with the zero momentum state (this is true even when interactions are introduced, and the full many-body ground state may no longer be described by a single-particle wavefunction). In a finite, non-uniform, interacting system, neither of these prescriptions apply. Instead, analysis of the OBDM gives the condensate fraction and corresponding state in terms of the largest eigenvalue of the OBDM and its corresponding eigenvector [20, 22, 23].

The OBDM, which characterizes the correlations between the particle density at points $\mathbf{r}$ and $\mathbf{r}'$ in a many-body quantum state, is given by [22]

$$\rho(\mathbf{r}, \mathbf{r}') = \langle \hat{\Psi}^\dagger(\mathbf{r}) \hat{\Psi}(\mathbf{r}') \rangle , \tag{8}$$

where $\hat{\Psi}(\mathbf{r})$ is the field operator that annihilates a single particle at the point $\mathbf{r}$. $\hat{\Psi}(\mathbf{r})$ can be expanded in terms of a set of single-particle wavefunctions $\phi_i(\mathbf{r})$ (the so called "natural orbitals") and the corresponding annihilation operators $\hat{a}_i$:

$$\hat{\Psi}(\mathbf{r}) = \sum_i \phi_i(\mathbf{r}) \hat{a}_i. \tag{9}$$

At $T = 0$, $\rho(\mathbf{r}, \mathbf{r}')$ is evaluated with respect to the N particle ground state wavefunction $\Psi_0(\mathbf{r}_1, \ldots, \mathbf{r}_N)$, which yields

$$\begin{aligned} \rho(\mathbf{r}, \mathbf{r}') &= \langle \Psi_0 | \hat{\Psi}^\dagger(\mathbf{r}) \hat{\Psi}(\mathbf{r}') | \Psi_0 \rangle \\ &= \sum_{ij} \phi_i^*(\mathbf{r}) \phi_j(\mathbf{r}') \langle \Psi_0 | \hat{a}_i^\dagger \hat{a}_j | \Psi_0 \rangle \\ &= \sum_i \phi_i^*(\mathbf{r}) \phi_i(\mathbf{r}') N_i \end{aligned} \tag{10}$$

where $\sum_i N_i = N$. Thus we see that the natural orbitals may be obtained as the eigenvectors of the OBDM in the position representation. The corresponding eigenvalues N_i give the occupation numbers of these natural orbitals in the many-body ground state wavefunction.

As a matter of notation, the natural orbital with highest occupation is given an index of 0, the next highest an index of 1, and so on, and we denote the fraction of particles occupying a given natural orbital by $n_i = N_i/N$. Any natural orbital which is occupied in the thermodynamic limit (i.e., which has nonzero n_i as N approaches infinity) can be interpreted as a condensate. For a typical

BEC, there is only one such natural orbital. When more than one natural orbital is occupied in the thermodynamic limit, the BEC is *fragmented* [15]. In either case, the total small population distributed among the other natural orbitals that vanishes in the thermodynamic limit is known as the *depletion* [24]. Hence, fragmentation and depletion can be distinguished in principle because the occupation of individual depleted orbitals goes to zero in the thermodynamic limit, but the fragmented states maintain a finite occupation. In practice, however, all of our work is done at finite N, so the distinction between fragmentation and depletion is ambiguous. Below, we make definitions for fragmentation and depletions parameters that, while arbitrary, are appropriate and useful for the double well system.

Intuitively, fragmentation in the double well can be related to the fluctuation of particles across the barrier. Suppose the barrier is very weak; then the ground state of the system is essentially the ground state of a single well, and there is no fragmentation. On the other hand, if the barrier is very strong, so that the wells can be thought of as isolated, then the particles in each well form independent condensates and the system is highly fragmented. Indeed, [7] predicted that the amount of fragmentation observed in a double well system would increase with the height of the barrier. Additionally, stronger interactions lead to reduced fluctuations, which constrains each atom in the system to occupy only one well. Thus, for strong repulsive interactions the condensate fragments into two independent condensates. This implies that fragmentation should also increase with interaction strength for a fixed barrier.

In analogy to the squeezing parameter S, we define fragmentation and depletion parameters, F and D. Reference [8] demonstrates that a condensate with G-fold degeneracy in its ground state can fragment into G parts, assuming low degeneracy ($G \approx 1$). From the energies listed in Table I, we see that the single-particle ground state has near-degeneracy (i.e., $G \to 2$) when L becomes large. Hence, it is reasonable to assume that, for the double well, at most two natural orbitals participate in fragmentation, and the rest, if occupied, constitute a very small amount of depletion (i.e., $n_0 + n_1 \approx 1$). This motivates us to define fragmentation and depletion parameters (F and D) as

$$F = 1 - |n_0 - n_1| \tag{11}$$

$$D = 1 - (n_0 + n_1). \tag{12}$$

With these definitions, a single condensate is represented by $F \approx D \approx 0$ and a doubly fragmented condensate is represented by $F \approx 1$ and $D \approx 0$. Because the OBDM in the two-mode model is a 2×2 matrix, there are only two natural orbitals and two occupation numbers for the system within that context. Hence, the depletion as defined here is necessarily zero for a two-mode description (see Sec. III A 4) but can be non-zero for an eight-mode description of the double well system.

III. DOUBLE WELL MODELS

Several simplified models have been proposed in attempts to reproduce the behavior of the interacting double well system while avoiding the difficulties associated with treating the interaction exactly. We describe several of these here.

The hard sphere interaction potential, Eq. (3), imposes the constraint that the wavefunction between two particles be 0 for $r_{ij} \leq a$. In the low energy limit and for $r_{ij} \geq a$, the wavefunction generated by the hard sphere potential is identical to the one that results from replacing this potential with a contact potential of the form [25, 26]

$$V_{int}(r_{jk}) = \frac{4\pi\hbar^2 a}{m}\delta(r_{jk}). \tag{13}$$

After doing so, the Hamiltonian for the system becomes

$$\hat{H} = \sum_{i=1}^{N}\left(\frac{\mathbf{p}_i^2}{2m} + V_{ext}(\mathbf{r}_i)\right) + \frac{4\pi\hbar^2 a}{m}\sum_{i<j}\delta(r_{jk}) \tag{14}$$

$$= \int d\mathbf{r}\,\hat{\Psi}^\dagger(\mathbf{r})\left(-\frac{\hbar^2}{2m}\nabla^2 + V_{ext}(\mathbf{r})\right)\hat{\Psi}(\mathbf{r}) + \frac{2\pi\hbar^2 a}{m}\int d\mathbf{r}\,\hat{\Psi}^\dagger(\mathbf{r})\hat{\Psi}^\dagger(\mathbf{r})\hat{\Psi}(\mathbf{r})\hat{\Psi}(\mathbf{r}), \tag{15}$$

where we have expressed it in both first and second quantized form. The field operator $\hat{\Psi}(\mathbf{r})$ can be expressed in terms of a complete basis of single-body states $\psi_i(\mathbf{r})$:

$$\hat{\Psi}(\mathbf{r}) = \sum_{i=1}^{\infty}\psi_i(\mathbf{r})\hat{a}_i. \tag{16}$$

Upon substituting, we find

$$\hat{H} = \sum_{i,j=1}^{\infty}\hat{a}_i^\dagger\hat{a}_j\epsilon_{ij} + a\sum_{i,j,k,l=1}^{\infty}\hat{a}_i^\dagger\hat{a}_j^\dagger\hat{a}_k\hat{a}_l\kappa_{ijkl}, \tag{17}$$

where

$$\epsilon_{ij} = \int d\mathbf{r}\,\psi_i^*(\mathbf{r})\left(-\frac{\hbar^2}{2m}\nabla^2 + V_{ext}(\mathbf{r})\right)\psi_j(\mathbf{r}) \tag{18}$$

$$\kappa_{ijkl} = \frac{2\pi\hbar^2}{m}\int d\mathbf{r}\,\psi_i^*(\mathbf{r})\psi_j^*(\mathbf{r})\psi_k(\mathbf{r})\psi_l(\mathbf{r}). \tag{19}$$

The (single particle) energy of a state i is given by ϵ_{ii}. For $i \neq j$, the ϵ_{ij} parameters characterize the tunneling between states i and j. The κ_{ijkl} parameters characterize the strength of two-body interactions. Note that these parameters are solely a function of the geometry of the potential.

The models we describe here amount to expanding $\hat{\Psi}(\mathbf{r})$ in a truncated basis of either two or eight single particle states.

A. Two-mode model

The two-mode model includes the lowest two single-particle energy states of the 3D double well

$$\psi_{g/e}(\mathbf{r}) = \psi_0(x,y)\phi_{0/1}(z), \tag{20}$$

where $\phi_0(z)$ and $\phi_1(z)$ are the ground and first excited states, respectively, of the 1D double well and

$$\psi_0(x,y) = \psi_0^{ho}(x)\psi_0^{ho}(y), \tag{21}$$

is the ground state of a 2D harmonic oscillator. As is conventional, we expand $\hat{\Psi}(\mathbf{r})$ in terms of linear combinations of these states that are localized in the left and right wells of the potential. These are

$$\psi_{l/r}(\mathbf{r}) = \psi_0(x,y)\phi_{l/r}(z), \tag{22}$$

where

$$\phi_{l/r}(z) = \frac{1}{\sqrt{2}}(\phi_0(z) \pm \phi_1(z)). \tag{23}$$

See Fig. 2 for examples of $\phi_{0/1}(z)$ and $\phi_{l/r}(z)$ for various potentials.

1. The two-mode Hamiltonian

By expanding $\hat{\Psi}(\mathbf{r})$ in terms of Eq. (22), the Hamiltonian Eq. (17) becomes

$$\begin{aligned}\hat{H} = {} & N(\Delta + a(N-1)\kappa_0)\hat{I} \\ & - 2a(\kappa_0 - 2\kappa_2)\hat{n}_l\hat{n}_r \\ & - (\delta/2 - 2a(N-1)\kappa_1)(\hat{a}_l^\dagger\hat{a}_r + \hat{a}_r^\dagger\hat{a}_l) \\ & + a\kappa_2(\hat{a}_l^\dagger\hat{a}_l^\dagger\hat{a}_r\hat{a}_r + \hat{a}_r^\dagger\hat{a}_r^\dagger\hat{a}_l\hat{a}_l),\end{aligned} \tag{24}$$

where $\delta = \epsilon_{ee} - \epsilon_{gg}$ (i.e., the energy difference between the excited and ground states), $\Delta = (\epsilon_{ee} + \epsilon_{gg})/2$ (i.e., the average energy of the excited and ground states, or equivalently, the energy of the left and right localized states), and the κ parameters are shorthand for various combinations of the κ_{ijkl}'s. In particular,

$$\begin{aligned}\kappa_0 &= \kappa_{llll} = \kappa_{rrrr} \\ &= (\kappa_{gggg} + \kappa_{eeee} + 6\kappa_{ggee})/4 \qquad (25) \\ \kappa_1 &= \kappa_{lllr} = \kappa_{lrrr} \\ &= (\kappa_{gggg} - \kappa_{eeee})/4 \qquad (26) \\ \kappa_2 &= \kappa_{llrr} \\ &= (\kappa_{gggg} + \kappa_{eeee} - 2\kappa_{ggee})/4. \qquad (27)\end{aligned}$$

Since the states are all real, $\phi_0(z)$ is even, $\phi_1(z)$ is odd, and $\phi_l(z) = \phi_r(-z)$, these are all of the distinct, nonzero κ_{ijkl} in the two-mode model. Note that both κ_0 and κ_2 are positive (since they are each the integral of the square of a function) while κ_1 can be positive or negative. We can estimate their relative size by defining a function $\beta(z)$ as the difference between the excited and ground state densities of the 1D double well:

$$\beta(z) = \phi_1^2(z) - \phi_0^2(z). \tag{28}$$

We can use $\beta(z)$ to reexpress κ_0, κ_1, and κ_2:

$$\begin{aligned}\kappa_0 = {} & 2\int_{-\infty}^{\infty}\phi_0^4(z)dz + 2\int_{-\infty}^{\infty}\phi_0^2(z)\beta(z)dz \\ & + \frac{1}{4}\int_{-\infty}^{\infty}\beta^2(z)dz \qquad (29)\end{aligned}$$

$$\kappa_1 = -\frac{1}{2}\int_{-\infty}^{\infty}\phi_0^2(z)\beta(z)dz - \frac{1}{4}\int_{-\infty}^{\infty}\beta^2(z)dz \tag{30}$$

$$\kappa_2 = \frac{1}{4}\int_{-\infty}^{\infty}\beta^2(z)dz. \tag{31}$$

In the case where $\phi_0^2(z) \approx \phi_1^2(z)$ (e.g., $L = 3\,a_{ho}$), $\beta(z) \ll 1$ and therefore $\kappa_0 \gg |\kappa_1| \gg \kappa_2$. Otherwise, the κ's are much closer to each other in value: $\kappa_0 > |\kappa_1| \approx \kappa_2$. See Table II for representative numerical values.

		κ $[\hbar\omega_{ho}/a_{ho}]$		
L $[a_{ho}]$	δ $[\hbar\omega_{ho}]$	κ_0	κ_1	κ_2
1	4.28×10^{-1}	5.74×10^{-2}	9.09×10^{-4}	6.79×10^{-3}
2	1.85×10^{-1}	5.31×10^{-2}	-1.22×10^{-3}	2.85×10^{-3}
3	3.02×10^{-3}	6.93×10^{-2}	-1.25×10^{-4}	1.35×10^{-6}

Table II. Values of the energy splitting δ and two-body interaction parameters κ_0, κ_1, and κ_2 for three trap geometries ($L = a_{ho}$, $2\,a_{ho}$, and $3\,a_{ho}$).

One can also write the two-mode Hamiltonian in terms of operators with the properties of angular momentum operators by defining [4]

$$\hat{J}_x = \frac{1}{2}(\hat{a}_l^\dagger\hat{a}_r + \hat{a}_r^\dagger\hat{a}_l) \tag{32}$$

$$\hat{J}_y = \frac{1}{2i}(\hat{a}_l^\dagger\hat{a}_r - \hat{a}_r^\dagger\hat{a}_l) \tag{33}$$

$$\hat{J}_z = \frac{1}{2}(\hat{n}_l - \hat{n}_r), \tag{34}$$

from which one finds

$$\hat{J}^2 = \frac{N}{2}\left(\frac{N}{2} + 1\right). \tag{35}$$

In this representation, the two-mode Hamiltonian (24) becomes

$$\begin{aligned}\hat{H} = {} & N(\Delta + a(3N+2)(\kappa_0 - \kappa_2)/2)\hat{I} \\ & - 2a(\kappa_0 - 3\kappa_2)\hat{J}_z^2 \\ & - (\delta - 4a(N-1)\kappa_1)\hat{J}_x \\ & + 4a\kappa_2\hat{J}_x^2.\end{aligned} \tag{36}$$

The natural basis for the two-mode Hamiltonian is a Fock bases $|n\rangle$, where $|n\rangle$ consists of the fully-symmetrized state with n particles in the $\psi_l(\mathbf{r})$ state

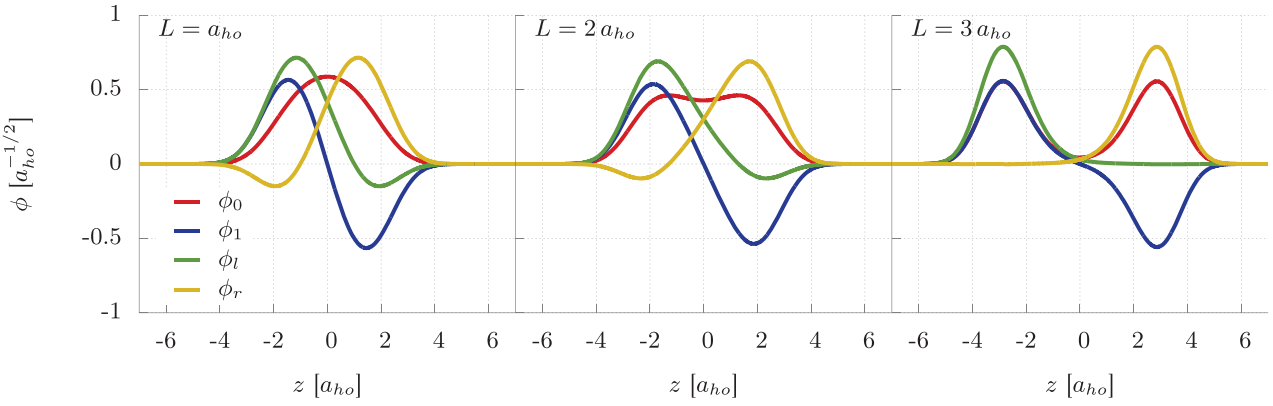

Figure 2. (Color online) The ground and first excited states of the z part of the double well potential (ϕ_0 and ϕ_1), and the left/right localized linear combinations of those states (ϕ_l and ϕ_r) for $\alpha = 4/81\,a_{ho}^{-2}$ and $L = a_{ho}$, $2\,a_{ho}$, and $3\,a_{ho}$.

and $N - n$ particles in the $\psi_r(\mathbf{r})$ state (i.e., $|n\rangle = |n\rangle_l\,|N-n\rangle_r$). Because the Fock states are also eigenstates of $\hat{J}^2$ and $\hat{J}_z$,

$$\hat{J}^2\,|n\rangle = \frac{N}{2}\left(\frac{N}{2}+1\right)|n\rangle \tag{37}$$

$$\hat{J}_z\,|n\rangle = \left(n - \frac{N}{2}\right)|n\rangle\,, \tag{38}$$

one can equivalently regard an N particle two-mode system as a spin-$N/2$ system, with the Fock states being the states of definite angular momentum projection in the z direction.

We can now interpret the terms of the two-mode Hamiltonian in the context of this Fock basis as follows, where we have omitted the coefficients of the operators for brevity:

$\hat{I}$: The energy that each Fock state has in common. We will ignore these terms when analyzing squeezing because doing so does not alter the ground state wavefunction of the system.

$-\hat{n}_l\hat{n}_r$: The state-dependent energy of each Fock state. This energy is lower the more evenly distributed the particles are, so $|N/2\rangle$ is the ground state for this term when considered alone.

$-(\hat{a}_l^\dagger\hat{a}_r + \hat{a}_r^\dagger\hat{a}_l)$: The energy due to transitions between Fock states that involve a single atom switching from the left to the right mode, or vice versa. This term depends on the scattering length a in addition to the usual dependence on the energy gap δ between the single-particle ground and excited states. The ground state for this part of the Hamiltonian alone is $\frac{1}{2^{N/2}}\sum_{n=0}^{N}\sqrt{\binom{N}{n}}\,|n\rangle$. Note that removing the minus sign in front of this term would leave the magnitude of the coefficients of this state unchanged but would cause their signs to alternate.

$\hat{a}_l^\dagger\hat{a}_l^\dagger\hat{a}_r\hat{a}_r + \hat{a}_r^\dagger\hat{a}_r^\dagger\hat{a}_l\hat{a}_l$: The energy due to transitions between Fock states that involve exactly two atoms switching from the left to the right mode, or vice versa. This term is due entirely to interparticle interactions. A Hamiltonian which includes only these terms can be rewritten in a block-diagonal form with two blocks, where each block involves either the even-numbered or the odd-numbered Fock states. Hence, the ground state can only involve either even or odd Fock states, but not both. We can confirm this reasoning through an explicit computation of the ground state of this term alone, which shows it to be $\frac{1}{2^{N/2}}\sum_{\substack{n=0\\ n\in\text{evens}}}^{N}\frac{\sqrt{n!(N-n)!}}{(n/2)!((N-n)/2)!}\,|n\rangle$.

2. *Nearly degenerate two-mode model*

Several previous studies [3–6] have analyzed the double well system under the two-mode model with the assumption that the two modes are nearly degenerate, that is, that $\phi_0^2(z) \approx \phi_1^2(z)$. Physically, this can be achieved by imposing a high and/or wide barrier. Mathematically, this amounts to assuming that $\kappa_{gggg} = \kappa_{ggee} = \kappa_{eeee}$ (so $\kappa_1 = \kappa_2 = 0$), thereby reducing the two-mode Hamiltonian to

$$\hat{H} = -\frac{\delta}{2}(\hat{a}_l^\dagger\hat{a}_r + \hat{a}_r^\dagger\hat{a}_l) - 2a\kappa_0\hat{n}_l\hat{n}_r \tag{39}$$

$$\hat{H} = -\delta\hat{J}_x - 2a\kappa_0\hat{J}_z^2. \tag{40}$$

This Hamiltonian has two natural limits. In the case where tunneling dominates ($a = 0$), the ground state is $\frac{1}{2^{N/2}}\sum_{n=0}^{N}\sqrt{\binom{N}{n}}\,|n\rangle$, from which one can compute $S = 0$. In the case where interactions dominate ($\delta = 0$), the ground state is $|N/2\rangle$ and $S = 1$. This behavior matches the argument made in Sec. II B.

The authors of [5] used the nearly degenerate two-mode model to compute an approximate analytical expression for the relative squeezing S. In the notation of

the present work, this is given by

$$S_{nd2} = 1 - 2^{1/3} \begin{cases} \left(\frac{1}{2^{2/3}+Na/a^*}\right)^{1/2} & a \le a^* N \\ N\left(\frac{a^*}{a}\right)^2 & a > a^* N \end{cases}, \quad (41)$$

where $a^* = \delta/2^{10/3}\pi\kappa_0$ is a function of the geometry of the double well. As a ranges between zero and infinity, Eq. (41) predicts that S_{nd2} will vary monotonically between 0 and 1 (apart from a discontinuity of $\mathcal{O}(N^{-3})$ at $a = a^*N$ that is an artifact of the approximations that went into the derivation of S_{nd2} [5]).

3. Exact two-mode model

The nearly degenerate two-mode model, while analytically tractable, misses many interesting features of the double well system. To identify these, we analyze the two-mode Hamiltonian (24) without making the assumption of near-degeneracy between the single-particle ground and first excited states. We note that [10] also studied the full two-mode Hamiltonian and [11] studied the two-mode Hamiltonian with $\kappa_2 = 0$, although neither of these studies investigated squeezing.

To proceed, we find the ground state of Eq. (24) via numerical diagonalization in the Fock representation without neglecting any terms. Because the size of the Hilbert space is $N+1$, this diagonalization is tractable for N up to several thousand. Given the coefficients c_n from the expansion of the ground state (i.e., $|\psi_{gs}\rangle = \sum_{n=0}^{N} c_n |n\rangle$), we can compute an analytical expression for the two-mode squeezing S_2:

$$\begin{aligned} S_2 &= S_{max}\left(1 - \frac{1}{N}\langle\psi_{gs}|(\hat{n}_l - \hat{n}_r)^2|\psi_{gs}\rangle\right) \\ &= S_{max}\left(1 - \frac{1}{N}\sum_{n=0}^{N}(N-2n)^2 c_n^2\right), \end{aligned} \quad (42)$$

with

$$S_{max} = \left(1 - 2\int_{-\infty}^{0} |\phi_l(z)|^2\, dz\right)^2. \quad (43)$$

S_{max} is the largest value of S_2 achievable for a given potential, and it is achieved only in the pure $|N/2\rangle$ state. S_{max} is also a function of the degree of degeneracy of the two modes: if they are exactly degenerate, then all of the probability for $\phi_l(z)$ is contained in the left well and $S_{max} = 1$. Otherwise, part of $\phi_l(z)$ extends into the right side of the potential (and vice versa for $\phi_r(z)$), and $S_{max} < 1$. Physically, this means that when the modes are not exactly degenerate there is a nonzero probability of measuring a difference in the number of particles between the two wells even in the $|N/2\rangle$ state. For $\alpha = 4/81\, a_{ho}^{-2}$, explicit evaluation of Eq. (43) yields values of $S_{max} = 0.704$, 0.820, and 0.999 for $L = a_{ho}$, $2\,a_{ho}$, and $3\,a_{ho}$, respectively; in other words, higher barriers lead to more potential for squeezing.

As we have seen previously, $c_n^2 = \frac{1}{2^N}\binom{N}{n}$ when $a = 0$, and hence $S_2 = 0$ for the non-interacting system. If the ground state is $|N/2\rangle$, then $c_{N/2} = 1$ (all other $c_i = 0$) and $S_2 = S_{max}$. From the above values of S_{max}, we therefore see that even within the two-mode model, the maximum possible relative squeezing is quite sensitive to the barrier height and is reduced as the height decreases. The inclusion of two-body interaction terms also influences the system: the results in Sec. IV A show that not only is $|N/2\rangle$ not the ground state in the $a \to \infty$ limit, but also that the squeezing does not necessarily increase monotonically as a function of a.

It is also interesting to note that in the completely degenerate case, $\hat{n}_l = \hat{L}$ and $\hat{n}_r = \hat{R}$, so that S_2 is then equal to S as defined in Eq. (7). One can thus interpret S_{max} as compensating for the fact that in the non-degenerate case (i.e., for realistic finite barrier heights), the operators in the two-mode Hamiltonian ($\hat{n}_l$ and $\hat{n}_r$) are not identical to $\hat{L}$ and $\hat{R}$, the operators that define squeezing (see Eq. (4)).

4. Fragmentation and depletion in the two-mode model

We can also study fragmentation in the two-mode model by expanding the OBDM (8) in terms of the modes (22) and diagonalizing it to find the occupation of the natural orbitals. In doing so, we find

$$\rho(\mathbf{r}, \mathbf{r}') = n_0\phi_0(\mathbf{r})\phi_0(\mathbf{r}') + n_1\phi_1(\mathbf{r})\phi_1(\mathbf{r}'), \quad (44)$$

where

$$n_{0/1} = \frac{1}{2} \pm \frac{1}{N}\sum_{n=0}^{N-1}\sqrt{(N-n)(n+1)}\, c_n c_{n+1}. \quad (45)$$

In other words, the natural orbitals are the single-particle ground and first excited states of the double well, and their occupations depend on the form of the ground state of the system. Using this result, we can express the fragmentation and depletion parameters (12) as

$$F = 1 - \frac{2}{N}\left|\sum_{n=0}^{N-1}\sqrt{(N-n)(n+1)}\, c_n c_{n+1}\right| \quad (46a)$$

$$D = 0. \quad (46b)$$

Because this model only has two modes, D must equal 0 by definition. For the maximally-squeezed state $|N/2\rangle$, we have $F = 1$ and the system is maximally fragmented. On the other hand, for the noninteracting ground state, the sum in this expression evaluates to $N/2$, and therefore $F = 0$ and there is no fragmentation. Note however that there is no general one-to-one relationship between the squeezing parameter S and the fragmentation parameter F in the two-mode model.

B. Eight-mode model

As an attempt to improve on the two-mode model, a recently-proposed eight-mode model [12] expands $\hat{\Psi}(\mathbf{r})$ in terms of the two modes (22) and six additional modes. We construct these additional modes using left- and right-localized linear combinations of the second and third double well excited states ($\phi_2(z)$ and $\phi_3(z)$):

$$\phi_{L/R}(z) = \frac{1}{\sqrt{2}}(\phi_2(z) \pm \phi_3(z)). \tag{47}$$

See Fig. 3 for examples of these states. We also use linear combinations of harmonic oscillator states with well-defined angular momentum in the z-direction:

$$\psi_{\pm}(x,y) = \frac{1}{\sqrt{2}}(\psi_0^{ho}(x)\psi_1^{ho}(y) \pm i\psi_1^{ho}(x)\psi_0^{ho}(y)). \tag{48}$$

All together, the eight modes are

$$\begin{aligned}
\psi_{100}^{l/r}(\mathbf{r}) &= \psi_0(x,y)\phi_{l/r}(z) \\
\psi_{210}^{l/r}(\mathbf{r}) &= \psi_0(x,y)\phi_{L/R}(z) \\
\psi_{21\pm1}^{l/r}(\mathbf{r}) &= \psi_{\pm}(x,y)\phi_{l/r}(z),
\end{aligned} \tag{49}$$

where we have introduced a set of three subscripts to distinguish the modes. If one chooses a potential such that the curvature at the well minima is roughly equal in the x, y, and z directions (as opposed to a pancake- or cigar-like geometry), then the subscripts on $\psi_{nlm}^{l/r}$ can be interpreted as the quantum numbers for a particle in a spherical potential [27]: n indexes the energy of the state and l and m index its angular momentum.

The modes in Eq. (49) are the modes used in [12], for a potential identical in form to ours. However, a subtlety can arise when one tries to use these modes to model double well potentials with certain geometries (i.e., with certain sets of values for the parameters α and L). Because the geometry of the double well determines the relative energies of the single particle states, it is possible to choose a geometry such that these eight modes are not the single-particle modes of lowest energy, in which case it would be more appropriate to expand the Hamiltonian in terms of whichever modes are the ones with lowest energy. Hence, to use these modes, one should choose geometries such that the eight states described here actually have the lowest energies. The geometries used in the current work have this property while at the same time also illustrating the behavior of the system over a wide range of barrier strengths. Table III lists the energies of the modes for our geometries.

As in the two-mode case, we use these eight modes to express the Hamiltonian in a Fock basis and diagonalize the resulting matrix, which we do not reproduce here. For N particles and M modes, the dimension of the Hilbert space is $\frac{(N+M-1)!}{N!(M-1)!}$, so the size of the matrix grows rapidly with N for $M = 8$. This restricts the practical usefulness of the eight-mode model to small N because of the computational cost of diagonalizing large matrices. However, the Hamiltonian has a block-diagonal form, with each block corresponding to a different value of m from $-l$ to l. The ground state has $m = 0$, so one can make the diagonalization process easier by only diagonalizing the $m = 0$ block. In this way, we were able to compute eight-mode model results for up to $N = 10$.

	Energy [$\hbar\omega_{ho}$]			
L [a_{ho}]	100	21±1	210	$V_{ext}(0)$
1	1.38	2.38	2.58	0.025
2	1.39	2.39	2.32	0.395
3	1.64	2.64	2.74	2

Table III. Energies of the 8 modes and the double well barrier, for $\alpha = 4/81\, a_{ho}^{-2}$ and various L.

One can in principle compute analytical expressions for the squeezing, fragmentation, and depletion parameters in the eight-mode model that are analogous to Eqs. (42), (46a), and (46b). However, these expression are complicated and not particularly illuminating. Instead, we will analyze the differences in these properties between the two models with numerical calculations in Sec. IV below.

IV. RESULTS & DISCUSSION

We present results for double well potentials with $\alpha = 4/81\, a_{ho}^{-2}$ and $L = a_{ho}$, $2\,a_{ho}$, and $3\,a_{ho}$. As discussed above, we chose these potentials so that we could study a range of barrier heights while staying in a regime where it is sensible to apply both the two-mode and eight-mode models.

A. Two-mode model results

We first present the nearly-degenerate and exact two-mode model results for squeezing and fragmentation.

1. *Squeezing*

In Fig. 4 we show the behavior of S as a function of a for a variety of particle numbers and in three different double well geometries for both the nearly degenerate two-mode model and the exact two-mode model. In general, the models agree well only for small values of a, and the deviations between them tend to grow with N. There are several notable features of the results in Fig. 4 that require detailed analysis. In particular, these are the lack of monotonicity (especially for low barriers) for S vs. a, the tendency of S to increases as the mode degeneracy increases (i.e., for higher barriers), and the tendency of S to decrease as a function of N for large a.

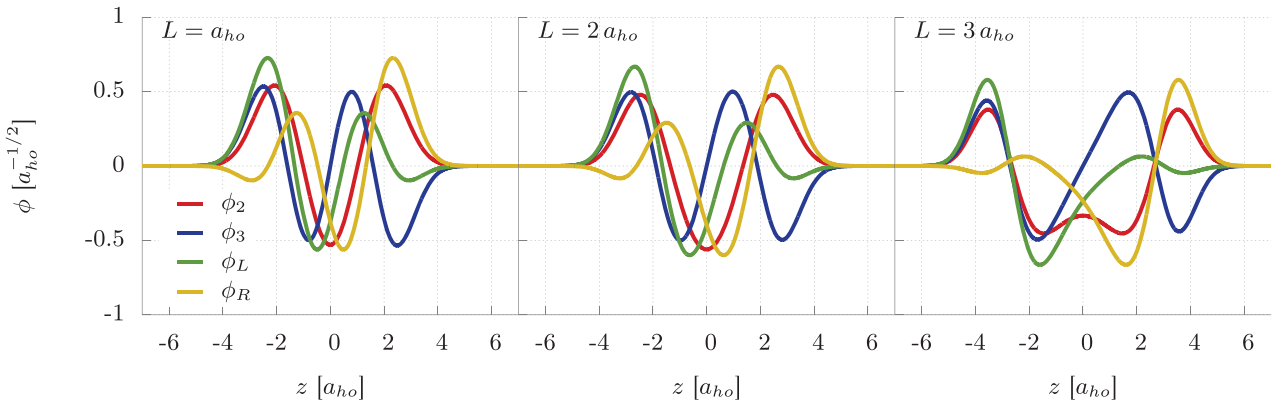

Figure 3. (Color online) The second and third excited states of the z part of the double well potential (ψ_2 and ψ_3), and the left/right localized linear combinations of those states (ψ_1^L and ψ_1^R) for $\alpha = 4/81\,a_{ho}^{-2}$ and $L = a_{ho}$, $2\,a_{ho}$, and $3\,a_{ho}$, from left to right.

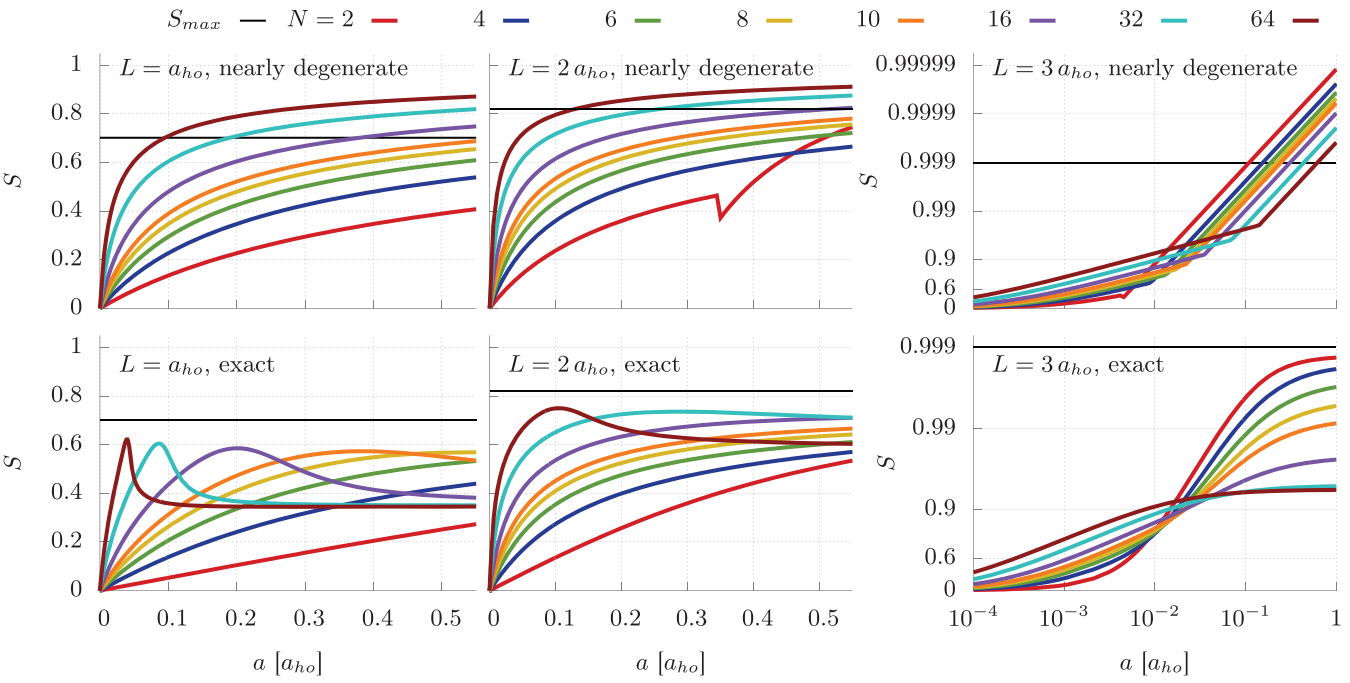

Figure 4. (Color online) Squeezing S vs. scattering length a for various particle number N between 2 and 64 for three different potentials ($L = a_{ho}$, $2\,a_{ho}$, and $3\,a_{ho}$ from left to right). The upper and lower plots are of S as computed in the nearly degenerate two-mode model (i.e., using Eq. (41)) and the exact two-mode model, respectively. All plots also indicate the value of S_{max} from Eq. (43).

The degree of squeezing is of course a reflection of the composition of the ground state. In Fig. 5, we visualize this composition by plotting the squared magnitude of the coefficients $c_n = \langle n|\psi_{ground}\rangle$ as a function of a for 8 and 64 particles and for potentials with $L = a_{ho}$, $2\,a_{ho}$, and $3\,a_{ho}$. The squeezing argument in Sec. II B would suggest that each of these plots should show a smooth transition from a binomial distribution centered at $n = N/2$ to sole occupancy of the $n = N/2$ state as a increases from 0. This is clearly not what happens for 64 particles: for $L = a_{ho}$ the ground state settles into a very wide "striped" pattern, with occupancy of every other Fock state, for $L = 2\,a_{ho}$ it settles into a different striped pattern, and for $L = 3\,a_{ho}$ it settles into a narrow but wider-than-one-state distribution. Even for 8 particles, the distribution narrows to the state $|4\rangle$ only for the highest barrier, $L = 3$, and the largest a values, $a \geq 0.1$. Based on the definition for S_2, Eq. (42), the width or "spread" of these patterns gives a sense of the degree of squeezing: narrower means more squeezing and vice versa. We can thereby see that the progression of these patterns is consistent with the trends seen in the

L $[a_{ho}]$	a^* $[a_{ho}]$	χ_1^*	χ_2
1	117.6	48.2	7.74×10^{-2}
2	−37.9	−38.8	3.01×10^{-2}
3	−6.0	−553.2	9.73×10^{-6}

Table IV. Values of a^*, χ_1^*, and χ_2 for $L = a_{ho}$, $2\,a_{ho}$, and $3\,a_{ho}$.

squeezing plots displayed in Fig. 4.

Ideally, one could simply use the expression for S in Eq. (42) to explain the observed trends. For example, the form of S_{max} implies that, in general, one should expect more squeezing for potentials with a higher degree of degeneracy between the two modes; this is supported by the data. However, there is no explicit analytical expression for the c_n's for the exact two-mode Hamiltonian that allows one to extract the dependence of S_2 on a and L.

We therefore study the ground state in different parameter regimes. Typically, the nearly-degenerate two-mode Hamiltonian, Eq. (39), has been described in terms of three regimes: Rabi, Josephson, and Fock (see, e.g., [21]). The Rabi regime is the one in which the two-body interactions are negligible compared with the effects of single-particle tunneling, whereas in the other two regimes the two-body interactions dominate. The Josephson and Fock regimes are further distinguished in that the interactions are so strong in the Fock regime that number fluctuations are suppressed (i.e., the ground state is $|N/2\rangle$) while in the Josephson regime there are still some fluctuations due to one-particle tunneling. These regimes are defined by the value of the dimensionless parameter $\chi = 4a\kappa_0/\delta$. The Rabi regime has $\chi \ll N^{-1}$, the Josephson regime has $N^{-1} \ll \chi \ll N$, and the Fock regime has $N \ll \chi$.

To make contact between these different regimes for the nearly-degenerate two mode model and the behavior of the exact two-mode system, we rewrite the full two-mode Hamiltonian as

$$\hat{H} = -(\hat{a}_l^\dagger \hat{a}_r + \hat{a}_r^\dagger \hat{a}_l) + \chi_1(a, N)\hat{H}', \tag{50}$$

where

$$\hat{H}' = -\hat{n}_l\hat{n}_r + \chi_2(\hat{a}_l^\dagger\hat{a}_l^\dagger\hat{a}_r\hat{a}_r + \hat{a}_r^\dagger\hat{a}_r^\dagger\hat{a}_l\hat{a}_l), \tag{51}$$

$$\chi_1(a, N) = \frac{a\chi_1^*}{a^* - a(N-1)}, \tag{52}$$

$$\chi_2 = \frac{\kappa_2}{2(\kappa_0 - 2\kappa_2)}, \tag{53}$$

and we have defined $a^* = \delta/4\kappa_1$ and $\chi_1^* = (\kappa_0 - 2\kappa_2)/\kappa_1$ for convenience. Both a^* and χ_1^* are functions solely of the geometry of the double well. For the geometries studied in this work, $\kappa_0 - 2\kappa_2 > 0$ (see Table II), so the signs of a^* and χ_1^* are the same as the sign of κ_1. See Table IV for representative numerical values for these parameters.

Because χ_1 reduces to χ when $\kappa_1 = \kappa_2 = 0$, the Hamiltonianin (50) reduces to Eq. (39) in the nearly degenerate limit, as it should. This motivates us to generalize the definitions of the three two-mode regimes that are defined for the nearly-degenerate two-mode model to the full two-mode system. As an example, recall that physically the Rabi regime is the one in which two-body interactions are negligible. Because χ_1 can be both positive or negative, this physical condition corresponds mathematically to both $0 < \chi_1 \ll N^{-1}$ and $0 > \chi_1 \gg -N^{-1}$ in Eq. (50). Hence, we define a Rabi-like regime as $|\chi_1| \ll N^{-1}$. Similarly, we define a Josephson-like regime as $N^{-1} \ll |\chi_1| \ll N$ and a Fock-like regime as $N \ll |\chi_1|$.

In Fig. 6 we schematically plot $|\chi_1|$ as a function of a for both positive and negative κ_1. For positive κ_1, we see that the system will have Rabi-, Josephson-, and Fock-like regimes for some range of interaction strength a, since $|\chi_1|$ diverges at $a = a^*/(N-1)$. For negative κ_1, the system will have a Rabi-like regime but may or may not have Josephson- or Fock-like regimes, depending on whether $|\chi_1^*| < N^{-1}$, $N^{-1} < |\chi_1^*| < N$, or $N < |\chi_1^*|$. In Fig. 7, we plot $|\chi_1|$ as a function of a for the same six sets of parameters that are depicted in Fig. 5; we also include the values of N and N^{-1} in the plots to make it clear where transitions between the three regimes occur. These transitions correspond to the vertical lines in Fig. 5 (see also the description in the caption to Fig. 5).

How close these regimes for the full two-mode system are to the "ideal" Rabi, Josephson, and Fock regimes defined in the nearly degenerate case depends on the value of χ_2. In Fig. 8, we plot the ground state of $\hat{H}'$ as a function of χ_2 for $N = 8$ and 64. The ground state progresses from $|N/2\rangle$ to a striped pattern as χ_2 increases. This comes about because $\hat{H}'$ can be rewritten in a block-diagonal form with two tridiagonal blocks, where each block involves either the even-numbered or the odd-numbered Fock states. Additionally, the form of $\hat{H}'$ invites an analogy between $\hat{H}'$ and Eq. (39) that allows us to identify $\chi_2 \ll N^{-1}$ as the regime in which $-\hat{n}_l\hat{n}_r$ dominates (and hence the ground state has true Rabi, Josephson, and Fock regimes) and $N \ll \chi_2$ as the regime in which two-body tunneling dominates. We note that there is an additional subtlety when $\chi_2 > 1$. The identification of χ_1 with χ depends on the two terms in $\hat{H}'$ having one coefficient less than 1 and one equal to 1, which does not hold for large χ_2. In that case, one should pull the factor of χ_2 out of $\hat{H}'$, and the Rabi-, Josephson-, and Fock-like regimes are defined instead by the size of the product $\chi_1\chi_2$.

Given this interpretation of χ_1 and χ_2, we can now understand the patterns in Fig. 9, where the ground state of Eq. (50) is plotted as a function of χ_1 for various values of χ_2 for $N = 8$ and 64. In the Rabi-like regime (small χ_1), the ground state is close to the binomial distribution of the one-body tunneling terms regardless of the size of χ_2. In the Fock-like regime, (large χ_1), the ground state varies from $|N/2\rangle$ to a wide striped pattern as χ_2 increases. The Josephson-like regime interpolates

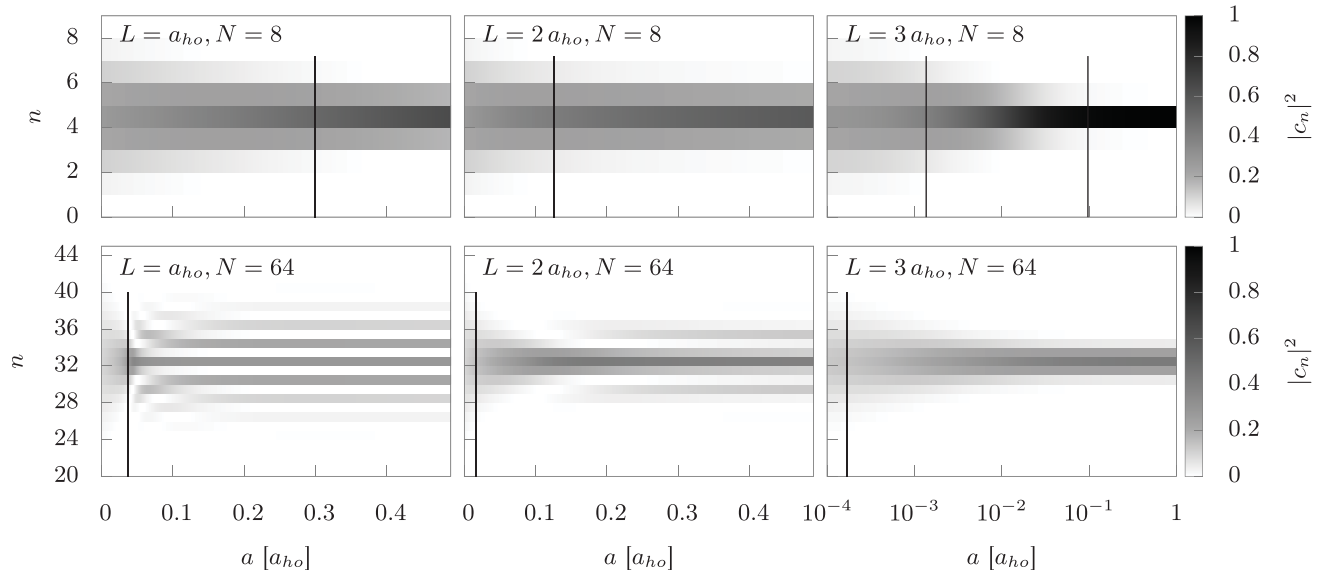

Figure 5. The components of the ground state ($c_n = \langle n|\psi_{ground}\rangle$) for the double well potential as a function of scattering length a as computed in the exact two-mode model for $N = 8$ (top row) and 64 (bottom row) for $L = a_{ho}$, $2\,a_{ho}$, and $3\,a_{ho}$ (left to right). The vertical lines indicate the boundaries between the Rabi-, Josephson-, and Fock-like regions, from left to right in each plot (although only the $L = 3\,a_{ho}$, $N = 8$ plot has a Fock-like regime visible in the plot). In addition to the indicated regimes, the $L = a_{ho}$, $N = 8$ plot has a Fock-like regime between $a = 9.03$ and 121 (and a Josephson-like regime thereafter) and the $L = a_{ho}$, $N = 64$ plot has a Fock-like regime between $a = 1.85$ and 1.98 (and a Josephson-like regime thereafter).

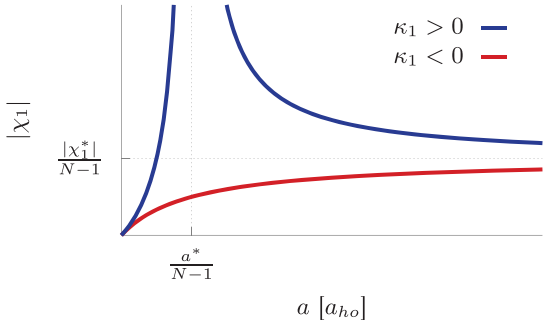

Figure 6. (Color online) Schematic plot of $|\chi_1|$ as a function of a for both positive and negative κ_1. For positive κ_1, $|\chi_1|$ diverges at $a^*/(N-1)$ and then asymptotes to $|\chi_1^*|/(N-1)$ from above; all three regimes (Rabi-, Josephson-, and Fock-like) are present for some range of a. For negative κ_1, $|\chi_1|$ asymptotes to $|\chi_1^*|/(N-1)$ from below, and there may or may not be Josephson- or Fock-like regimes depending on the size of $|\chi_1^*|/(N-1)$ compared with N and N^{-1}.

between the other two, with a narrow "neck" where the binomial and striped patters touch. Recall that S varies like the width of these distributions (recall (Eq. (42)), so the neck corresponds to a peak in S.

With this understanding, we can now interpret the trends in two-mode data seen in Figs. 4 and 5. The closer we are to the degenerate two-mode system (i.e., larger L, smaller κ_2, and smaller χ_2), the closer the ground state will be to $|N/2\rangle$ (as opposed to a striped state) for large a. This implies that there will generally be more squeezing with increased degeneracy. Likewise, the closer the system is to the degenerate limit, the more likely that S varies monotonically with a: because the large-a state is narrower, the neck in the Josephson-like regime (and hence the peak in S) will be less pronounced or non-existent. Finally, for very large a, $\chi_1 = \chi_1^*/(N-1)$. As N increases, this quantity decreases, and therefore the Hamiltonian becomes increasingly dominated by the one-body tunneling terms, which have a wide distribution of Fock states in the ground state. Hence, we expect S to decrease with increasing N for very large a.

2. *Fragmentation and Depletion*

To investigate fragmentation in the exact two-mode model, we plot the fragmentation parameter F as a function of a for three geometries in Fig. 10. Recall that the larger F, the more fragmentation there is in the system. Fig. 10 shows that in general, fragmentation increases with a. The exception occurs for low L and large a, for which n_1 becomes greater than n_0, and therefore the amount of squeezing drops from a maximum of 1. However, the most notable feature of these plots is that for low barriers ($L = a_{ho}$), systems with larger N experience much more fragmentation than systems with smaller N, whereas the opposite is true for systems with high barriers ($L = 3\,a_{ho}$). Equivalently, for small N, increasing the barrier height increases the amount of fragmentation,

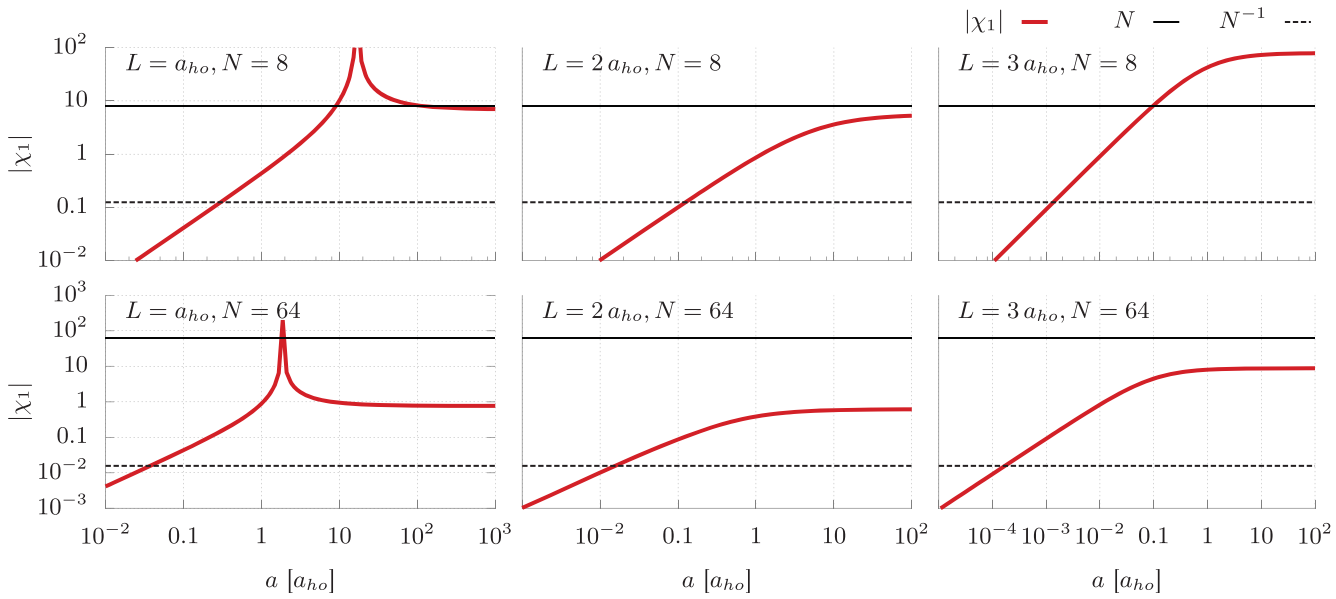

Figure 7. (Color online) The value of the parameter $|\chi_1|$ from Hamiltonian (50) as a function of a for $L = a_{ho}$, $2\,a_{ho}$, and $3\,a_{ho}$ and $N = 8$ and 64. Also indicated in each plot are the values of N (solid horizontal line) and N^{-1} (dotted horizontal line). The system is in a Rabi-like regime $|\chi_1|$ is below the dotted line, a Josephson-like regime when $|\chi_1|$ is between the two lines, and a Fock-like regime when $|\chi_1|$ is above the solid line. We see that while the Rabi-like regime must always be present (since $\chi_1 = 0$ for $a = 0$), the other two need not be.

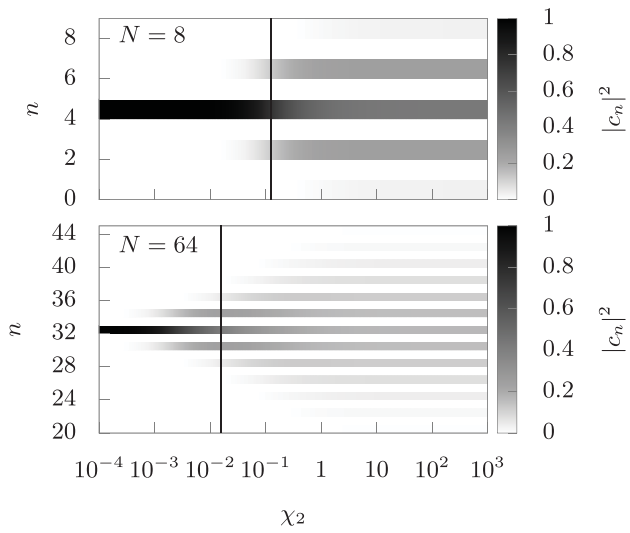

Figure 8. The components of the ground state of $\hat{H}'$ as a function of χ_2 for $N = 8$ and 64. The vertical line indicates the location of $\chi_2 = N^{-1}$, which forms the boundary between the values of χ_2 for which true Rabi, Josephson, and Fock regimes are found (to the left) and not found (to the right).

while for large N, increasing the barrier height decreases the amount of fragmentation.

We can understand these trends by examining the structure of the ground state illustrated in Fig. 5. First, consider the high barrier limit ($L = 3\,a_{ho}$). Based on the arguments above, we expect the ground state to be narrower (closer to $|N/2\rangle$) for smaller N. From the analytic form of F given in Eq. (46a), we see that the terms in the sum depend on $c_i c_{i+1}$, i.e. the product of two adjacent c_i's; the smaller the products, the more fragmentation there is. In general, then, we expect a narrower ground state to have more fragmentation, because it will have smaller $c_i c_{i+1}$ products than a wider ground state (indeed, if the ground state is $|N/2\rangle$, all of the $c_i c_{i+1}$ products are zero). Hence, fragmentation decreases with N at large a for $L = 3\,a_{ho}$.

For low barriers ($L = a_{ho}$), the situation is different. As N increases, the ground state widens (as with $L = 3\,a_{ho}$), but it does so by developing a striped pattern. Despite the fact that the pattern is wide for large N, the striping will cause the $c_i c_{i+1}$ products to be small because for each pair of adjacent c_i's, one of them will be close to zero. Hence, there will be more fragmentation for large N than for small N at large a for $L = 3\,a_{ho}$.

The fragmentation pattern in the intermediate barrier regime ($L = 2\,a_{ho}$) is clearly a crossover between the low and high barrier situations.

B. Eight-mode model results

We now present the eight-mode model results for squeezing and fragmentation.

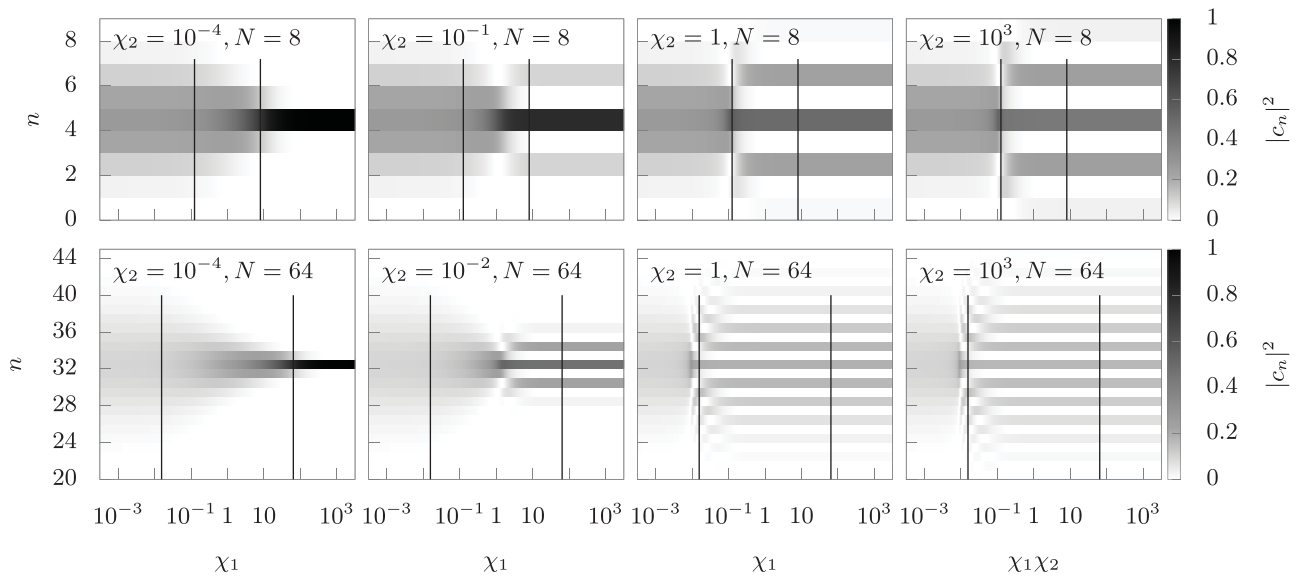

Figure 9. The components of the ground state of Eq. (50) as a function of χ_1 (or $\chi_1\chi_2$) for $N = 8$ and 64 and for a variety of χ_2. The vertical lines indicate the boundaries between the Rabi-, Josephson-, and Fock-like regimes, from left to right in each plot.

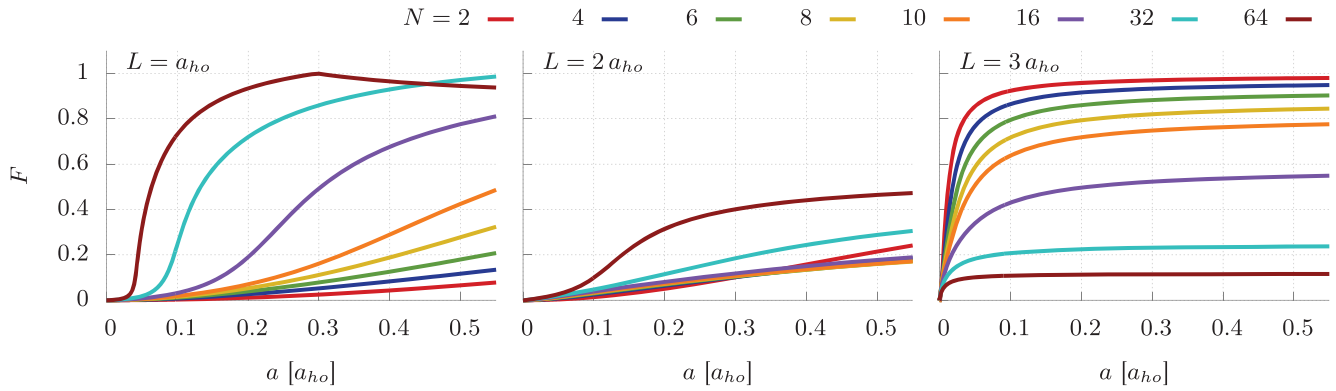

Figure 10. (Color online) The fragmentation F vs. scattering length a for various particle number N between 2 and 64 for three different potentials ($L = a_{ho}$, $2\,a_{ho}$, and $3\,a_{ho}$, from left to right) in the exact two-mode model. Because there are only two modes in this model, the depletion parameter D equals 0.

1. *Squeezing*

In Fig. 11 we show the behavior of S for the eight-mode model as a function of a for a variety of particle numbers and in three different double well geometries for the eight-mode model. We do not go beyond 10 particles because of the severe computational cost of diagonalizing the resulting Hamiltonian (see Sec. III B). For the particle numbers for which we do have data, the squeezing behavior for the low barriers ($L = a_{ho}$ and $2\,a_{ho}$) looks qualitatively similar to the equivalent cases in the nearly degenerate and exact two-mode models (compare with Fig. 4). However, for $L = 3\,a_{ho}$ we see qualitatively different behavior: here the squeezing has a maximum. We would like to account for this behavior, despite the fact that the eight-mode Hamiltonian cannot be analytically analyzed as easily as the two-mode Hamiltonian because of its complexity (i.e., because the eight-mode equivalent to Eq. 24 is composed of many more terms with additional operators and parameters).

One way to do this is to look at the composition of the ground state with plots analogous to Fig. 5. However, because the Hilbert space for the eight-mode model is so large, it is not useful to plot the contribution to the ground state of each individual Fock state. Instead, we sum the contributions of all Fock states for which the difference in n_l and n_r is the same, regardless of which exact modes are occupied; this representation is shown in Fig. 12. By comparing Fig. 11 and Fig. 12, we see that a narrower distribution corresponds to more squeezing (as in the two-mode model), and that the maximum in the

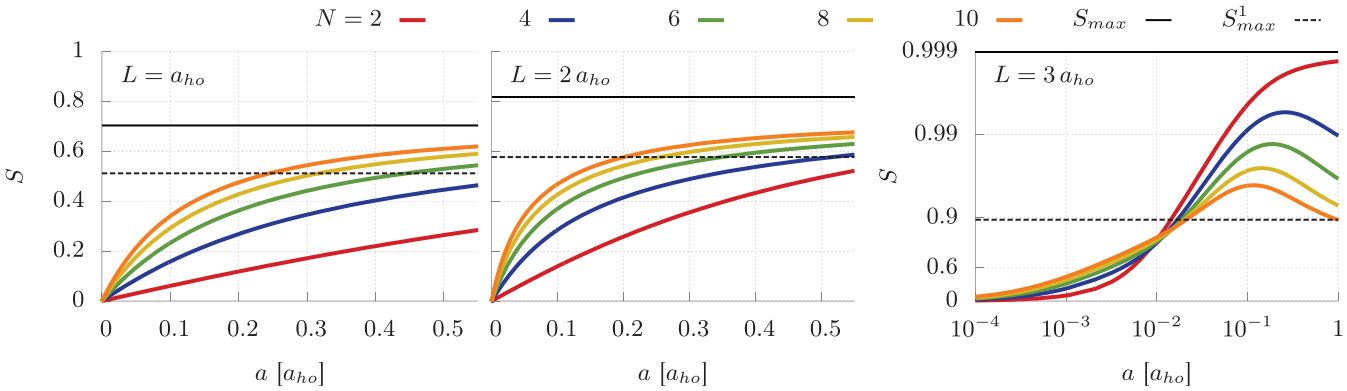

Figure 11. (Color online) Squeezing S vs. scattering length a for various particle number N between 2 and 10 for three different potentials ($L = a_{ho}$, $2\,a_{ho}$, and $3\,a_{ho}$, from left to right) in the eight-mode model. The horizontal lines indicate the values of S_{max} and S^1_{max}.

$L = 3\,a_{ho}$ squeezing data corresponds to a narrow neck in the state distribution.

It is also useful to consider the implications of the eight-mode analog to the quantity S_{max}, Eq. (43), which puts a constraint on the maximum amount of squeezing possible for the two-mode model in a given double well potential. Recall that S_{max} measures the fraction of a left or right localized state on the "wrong" side of $z = 0$; the more "spillover," the smaller S_{max}. In general, the modes that involve $\phi_{L/R}(z)$ (with $nlm = 210$) will have more spillover than the other six states, which all involve $\phi_{l/r}(z)$ (see Eq. (49) and compare Figs. 2 and 3). This motivates us to define S^1_{max},

$$S^1_{max} = \left(1 - 2\int_{-\infty}^{0} |\phi_L(z)|^2\, dz\right)^2, \qquad (54)$$

as a measure of the spillover of the $nlm = 210$ modes; this quantity is analogous to S_{max} for the $nlm = 100$ and 21 ± 1 modes. For $L = a_{ho}$, $2\,a_{ho}$, and $3\,a_{ho}$, $S_{max} = 0.704$, 0.820, and 0.999 and $S^1_{max} = 0.512$, 0.577, and 0.895, respectively (these values are included in Fig. 11). Both S_{max} and S^1_{max} increase with L, so there is more potential for squeezing for higher barriers. However, note that $S^1_{max} < S_{max}$ for each L: this implies that the 210 modes have less potential for squeezing than the other modes. Hence, by analogy with the exact two mode analysis (see the discussion after Eq. (43)), we expect that a ground state will have less squeezing, other things being equal, if it is dominated by the 210 modes than if it is dominated by the others. In other words, Fock states with a given difference between n_l and n_r will contribute less to squeezing if they are dominated by the 210 modes because these modes have more spillover across $z = 0$.

In Fig. 13, we plot the fraction of particles in the eight-mode model ground state that are in the 210 modes. For the largest a plotted, that fraction reaches as high as 8 percent, with larger fractions for larger N. This is reasonable: in general, the repulsive interaction between the atoms drives them away from each other, and in an eight-mode model, one way that the atoms can avoid each other is by occupying modes with different values of m. Hence, we expect that, for a given a, increasing the number of particles in the system will result in a larger fraction of them occupying the 210 modes. The occupation of these modes can then reduce the amount of squeezing via the spillover mechanism described above.

2. *Fragmentation and Depletion*

In Fig. 14, we plot the fragmentation parameter F and depletion parameter D, Eq. (12), as a function of scattering length a in the eight-mode model for a variety of particle numbers and double well geometries. The main qualitative differences between these prediction and those of the two-mode model in Fig. 10 are that the eight-mode states exhibit less fragmentation and more depletion.

Recall that F and D are defined in terms of n_0 and n_1, the occupation numbers of the first two natural orbitals (see Eq. (12)). In the two-mode model, these are the only two occupation numbers, so there is no depletion. In the eight-mode model, there are eight natural orbitals to occupy. The fact that there is less fragmentation and simultaneously more depletion in the eight-mode case implies that the occupation of the orbitals is spread out among more than just the first two, but also that n_0 is larger relative to n_1 in the eight-mode case than in the two-mode case. This is not particularly surprising. In the two-mode case, the only way to reduce n_0 is to increase n_1. However, because the eight-mode states can occupy the other six natural orbitals, a reduction in n_0 can be compensated by an increase in any of n_1 through n_7. Hence, conditions that would have led to pure fragmentation in the two-mode case leads to less fragmentation with some depletion in the eight-mode case.

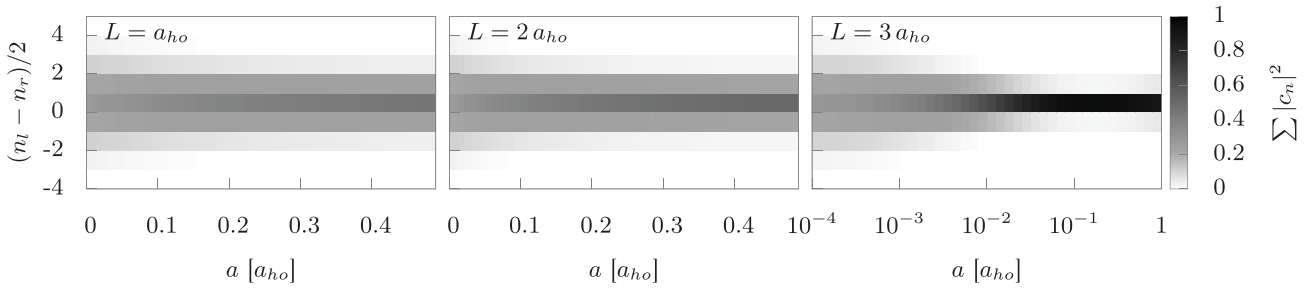

Figure 12. A representation of the ground state for the double well potential as a function of scattering length a as computed in the eight-mode model for $N = 8$ and various L (a_{ho}, $2\,a_{ho}$, and $3\,a_{ho}$, from left to right). The quantity plotted is the sum of $|c_n|^2$ for the components of the ground state that have a given value for the difference between the number of particles in left and right modes.

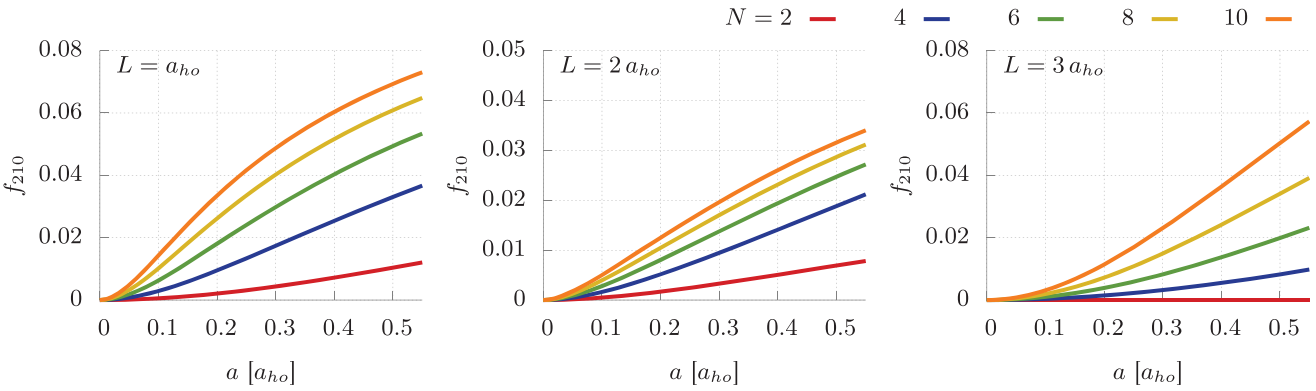

Figure 13. (Color online) Fraction f_{210} of particles in the 210 modes of the eight-mode model as a function of the scattering length a for various particle number N between 2 and 10 and for three different potentials ($L = a_{ho}$, $2\,a_{ho}$, and $3\,a_{ho}$, from left to right). The total fraction of particles in the 100 and 21 ± 1 modes (not shown) is given by $1 - f$.

V. CONCLUSION

In this work, we have made a detailed theoretical study of the squeezing and fragmentation exhibited by the ground state of an ultracold, bosonic atomic gas in a three-dimensional double well trap. While these properties have been studied previously in the context of two-mode models, we have greatly extended this analysis here by more deeply studying the two-mode model and by investigating squeezing and fragmentation phenomena in a recently-proposed eight-mode model. We have generalized the definitions of squeezing, fragmentation, and depletion to any finite basis representation of eigenstates for general double well potentials with variable barrier height. The generalized definition of squeezing shows clearly how the squeezing in a double well with finite barrier is dependent on the overlap between left- and and right-localized states, via the parameter S_{max}.

Previous studies, often conducted with a restricted two-mode model that is relevant only when the barrier is strong and therefore and the modes nearly degenerate, predicted that squeezing should monotonically increase with a and that fragmentation should monotonically increase with barrier strength. Instead, by including all possible contributions to the two-mode Hamiltonian, we find much more rich behavior, with the following characteristics:

- Squeezing is not necessarily monotonic with a, especially for weak barriers.
- For a given N, squeezing tends to increase with barrier strength.
- For a given barrier strength, squeezing tends to decrease with N for large a.
- For fixed a, fragmentation tends to increase with N for weak barriers, whereas fragmentation tends to decrease with N for strong barriers.

These trends can be explained by understanding how a, N, and the double well geometry parameters influence the relative importance of the terms in the exact two-mode Hamiltonian, and therefore change the nature of the ground state. A key parameter that characterizes these changes is $\chi_1(a, N)$, Eq. (52), which defines different regimes analogous to the Rabi, Josephson, and Fock regimes of the ideal, nearly-degenerate two mode model. With this, we may distinguish the following trends:

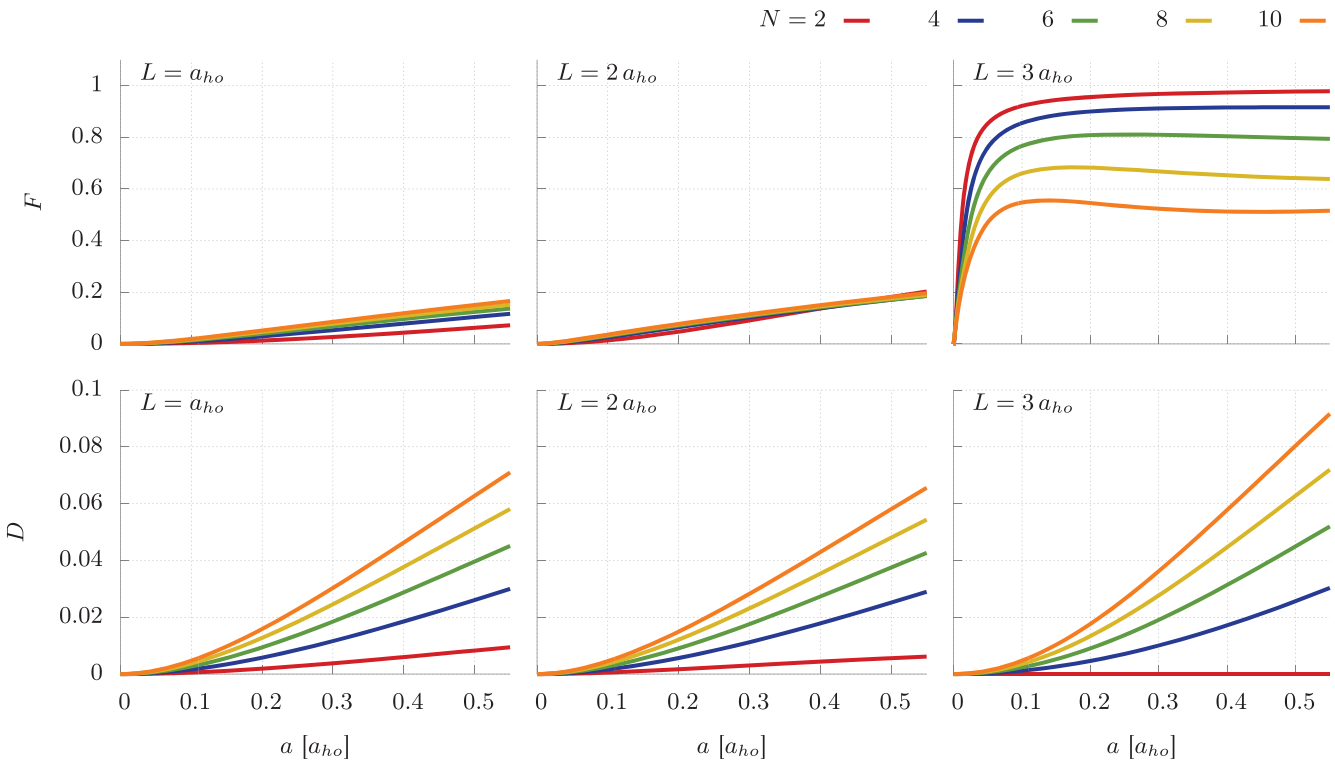

Figure 14. (Color online) The fragmentation F (top) and depletion D (bottom) vs. scattering length a for various particle number N between 2 and 10 for three different potentials ($L = a_{ho}$, $2\,a_{ho}$, and $3\,a_{ho}$, from left to right) in the eight-mode model.

- Weak interactions ($|\chi_1| \ll N^{-1}$) correspond to a ground state close to the binomially-distributed non-interacting ground state, for which both squeezing and fragmentation are very close to zero. This is true regardless of the shape of the barrier.
- A strong barrier ($\chi_2 \ll N^{-1}$) with strong interactions ($|\chi_1| \gg N$) corresponds to a ground state close to $|N/2\rangle$, for which both squeezing and fragmentation are large.
- A weak barrier ($\chi_2 \gg N$) with strong interactions ($|\chi_1| \gg N$) corresponds to a striped ground state, for which squeezing and fragmentation are both small, but not as small as the binomially-distributed state.
- Increasing N tends to increase the relative "width" of the ground state, i.e., the number of Fock states around $|N/2\rangle$ with significant contribution to the ground state.

Finally, we investigated squeezing, fragmentation, and depletion in the eight-mode ground state. Compared with the two-mode ground state, we found that the eight mode ground state

- exhibits less squeezing, especially for $L = 3\,a_{ho}$,
- exhibits a maximum in S vs. a for $L = 3\,a_{ho}$, and
- exhibits less fragmentation and more depletion.

Physically, these effects can be understood as a consequence of the occupation of modes in the $n = 2$ energy level in addition to the two-mode model's $n = 1$ modes. Because some of the $n = 2$ modes spread into the "wrong" well more so than the $n = 1$ modes, they lead to greater particle fluctuations across the barrier for the same value of $N_l - N_r$. Hence, to the extent that they are occupied in the ground state, those $n = 2$ modes will tend to suppress both squeezing and fragmentation in eight-mode ground states relative to two-mode ground states, . The presence of a maximum in the squeezing parameter comes about because of a competition between this effect and the usual suppression of particle fluctuations that comes about because of increasing the scattering length a. Finally, the presence of more than two natural orbitals in the eight-mode model allows for non-zero depletion when the "extra" modes are occupied, as opposed to the two-mode model in which depletion as we have defined it is not possible.

VI. ACKNOWLEDGEMENTS

This research was supported by the National Science Foundation and by the UC Lab Fees Research Program under a grant to the University of California,

Berkeley and Lawrence Livermore National Laboratory. J.D. acknowledges work performed under the auspices of the U.S. Department of Energy by Lawrence Livermore National Laboratory under Contract No. DE-AC52-07NA27344. K.B.W and J.C. also thank the Kavli Institute for Theoretical Physics for hospitality and for supporting this research in part by the National Science Foundation Grant No. PHY11-25915.

[1] K. B. Davis, M.-O. Mewes, M. R. Andrews, N. J. van Druten, D. S. Durfee, D. M. Kurn, and W. Ketterle, Phys. Rev. Lett. **75**, 3969 (1995).
[2] M. H. Anderson, J. R. Ensher, M. R. Matthews, C. E. Wieman, and E. A. Cornell, Science **269**, 198 (1995).
[3] K. W. Mahmud, J. N. Kutz, and W. P. Reinhardt, Phys. Rev. A **66**, 063607 (2002).
[4] G. J. Milburn, J. Corney, E. M. Wright, and D. F. Walls, Phys. Rev. A **55**, 4318 (1997).
[5] J. Javanainen and M. Y. Ivanov, Phys. Rev. A **60**, 2351 (1999).
[6] C. Bodet, J. Estève, M. K. Oberthaler, and T. Gasenzer, Phys. Rev. A **81**, 063605 (2010).
[7] R. W. Spekkens and J. E. Sipe, Phys. Rev. A **59**, 3868 (1999).
[8] E. J. Mueller, T.-L. Ho, M. Ueda, and G. Baym, Phys. Rev. A **74**, 033612 (2006).
[9] K. Sakmann, A. I. Streltsov, O. E. Alon, and L. S. Cederbaum, Phys. Rev. A **84**, 053622 (2011).
[10] D. Ananikian and T. Bergeman, Phys. Rev. A **73**, 013604 (2006).
[11] X. Jia, W. Li, and J. Q. Liang, Phys. Rev. A **78**, 023613 (2008).
[12] M. A. García-March, D. R. Dounas-Frazer, and L. D. Carr, Phys. Rev. A **83**, 043612 (2011).
[13] J. A. Dunningham, K. Burnett, and S. M. Barnett, Phys. Rev. Lett. **89**, 150401 (2002).
[14] J. A. Dunningham and K. Burnett, Phys. Rev. A **70**, 033601 (2004).
[15] P. Nozières and D. Saint James, J. Phys. France **43**, 1133 (1982).
[16] A. I. Streltsov, L. S. Cederbaum, and N. Moiseyev, Phys. Rev. A **70**, 053607 (2004).
[17] A. D. Jackson, G. M. Kavoulakis, and M. Magiropoulos, Phys. Rev. A **78**, 063623 (2008).
[18] J. C. Corbo, J. L. DuBios, and K. B. Whaley, "Squeezed and fragmented states of strongly interacting bosons in a double well. Part II: Quantum monte carlo simulations," Submitted.
[19] Y. Shin, M. Saba, T. A. Pasquini, W. Ketterle, D. E. Pritchard, and A. E. Leanhardt, Phys. Rev. Lett. **92**, 050405 (2004).
[20] O. Penrose and L. Onsager, Phys. Rev. **104**, 576 (1956).
[21] A. J. Leggett, Rev. Mod. Phys. **73**, 307 (2001).
[22] P.-O. Löwdin, Phys. Rev. **97**, 1474 (1955).
[23] T. D. Lee, K. Huang, and C. N. Yang, Phys. Rev. **106**, 1135 (1957).
[24] N. Bogoliubov, Изв. АН СССР, Сер. физ. (Bull. Acad. Sci. USSR, Phys.) **11**, 77 (1947).
[25] E. Fermi, Ricerca Sci. **7**, 13 (1936).
[26] G. Breit, Phys. Rev. **71**, 215 (1947).
[27] C. P. Friedman and E. F. Taylor, Am. J. Phys. **39**, 1073 (1971).